




# Dynamic contrast-enhanced MRI perfusion quantification in hepatocellular carcinoma: comparison of gadoxetate disodium and gadobenate dimeglumine

Daniel Stocker<sup>1,2</sup> · Stefanie Hectors<sup>1,3</sup> · Octavia Bane<sup>1,3</sup> · Naik Vietti-Violi<sup>1,4</sup> · Daniela Said<sup>1,5</sup> · Paul Kennedy<sup>1,3</sup> · Jordan Cuevas<sup>1,3</sup> · Guilherme M. Cunha<sup>6</sup> · Claude B. Sirlin<sup>6</sup> · Kathryn J. Fowler<sup>6</sup> · Sara Lewis<sup>1,3</sup> · Bachir Taouli<sup>1,3</sup> 

Received: 27 February 2021 / Revised: 22 April 2021 / Accepted: 11 May 2021 / Published online: 27 May 2021  
© European Society of Radiology 2021

## Abstract

**Objectives** (1) To assess the quality of the arterial input function (AIF) during dynamic contrast-enhanced (DCE) MRI of the liver and (2) to quantify perfusion parameters of hepatocellular carcinoma (HCC) and liver parenchyma during the first 3 min post-contrast injection with DCE-MRI using gadoxetate disodium compared to gadobenate dimeglumine (Gd-BOPTA) in different patient populations.

**Methods** In this prospective study, we evaluated 66 patients with 83 HCCs who underwent DCE-MRI, using gadoxetate disodium (group 1,  $n = 28$ ) or Gd-BOPTA (group 2,  $n = 38$ ). AIF qualitative and quantitative features were assessed. Perfusion parameters (based on the initial 3 min post-contrast) were extracted in tumours and liver parenchyma, including model-free parameters (time-to-peak enhancement (TTP), time-to-washout) and modelled parameters (arterial flow ( $F_a$ ), portal venous flow ( $F_p$ ), total flow ( $F_t$ ), arterial fraction, mean transit time (MTT), distribution volume (DV)). In addition, lesion-to-liver contrast ratios (LLCRs) were measured. Fisher's exact tests and Mann-Whitney  $U$  tests were used to compare the two groups.

**Results** AIF quality, modelled and model-free perfusion parameters in HCC were similar between the 2 groups ( $p = 0.054$ – $0.932$ ). Liver parenchymal flow was lower and liver enhancement occurred later in group 1 vs group 2 ( $F_p$ ,  $p = 0.002$ ;  $F_t$ ,  $p = 0.001$ ; TTP, MTT, all  $p < 0.001$ ), while there were no significant differences in tumour LLCR (max. positive LLCR,  $p = 0.230$ ; max. negative LLCR,  $p = 0.317$ ).

**Conclusion** Gadoxetate disodium provides comparable AIF quality and HCC perfusion parameters compared to Gd-BOPTA during dynamic phases. Despite delayed and decreased liver enhancement with gadoxetate disodium, LLCRs were equivalent between contrast agents, indicating similar tumour conspicuity.

## Key Points

- Arterial input function quality, modelled, and model-free dynamic parameters measured in hepatocellular carcinoma are similar in patients receiving gadoxetate disodium or gadobenate dimeglumine during the first 3 min post injection.
- Gadoxetate disodium and gadobenate dimeglumine show similar lesion-to-liver contrast ratios during dynamic phases in patients with HCC.
- There is lower portal and lower total hepatic flow and longer hepatic mean transit time and time-to-peak with gadoxetate disodium compared to gadobenate dimeglumine.

**Keywords** Liver neoplasms · Carcinoma, hepatocellular · Magnetic resonance imaging · Gadoxetate · Gadobenate dimeglumine

✉ Bachir Taouli  
bachir.taouli@mountsinai.org

<sup>1</sup> BioMedical Engineering and Imaging Institute, Icahn School of Medicine at Mount Sinai, New York, NY, USA

<sup>2</sup> Institute of Diagnostic and Interventional Radiology, University Hospital Zurich and University of Zurich, Zurich, Switzerland

<sup>3</sup> Department of Diagnostic, Molecular and Interventional Radiology, Icahn School of Medicine at Mount Sinai, 1470 Madison Avenue, New York, NY 10029, USA

<sup>4</sup> Department of Radiology, Lausanne University Hospital, Lausanne, Switzerland

<sup>5</sup> Department of Radiology, Universidad de los Andes, Santiago, Chile

<sup>6</sup> Liver Imaging Group, Radiology, University of California-San Diego, San Diego, CA, USA

## Abbreviations

AIF	Arterial input function
ART	Arterial fraction
[CA]	Contrast agent concentration
DCE-MRI	Dynamic contrast-enhanced magnetic resonance imaging
DV	Distribution volume
$F_a$	Arterial flow
$F_p$	Portal flow
Gd-BOPTA	Gadobenate dimeglumine
HBP	Hepatobiliary phase
HCC	Hepatocellular carcinoma
ICC	Intra-class correlation coefficient
IQR	Interquartile range
IR-LL	$T_1$ -weighted inversion recovery Look–Locker
LI-RADS	Liver Imaging Reporting and Data System
LLCR	Lesion-to-liver contrast ratio
MTT	Mean transit time
ROI	Region of interest
SD	Standard deviation
SI	Signal intensity

## Introduction

Imaging plays a key role in the diagnosis and staging of hepatocellular carcinoma (HCC) and an imaging-based diagnosis of HCC is accepted by several international guidelines [1–3]. The latest versions of the Liver Imaging Reporting and Data System (LI-RADS), published in 2018, considers the use of extracellular and hepatobiliary contrast agents in their diagnostic algorithms [4]. Both gadoxetate disodium (subsequently referred to as gadoxetate) and gadobenate dimeglumine (Gd-BOPTA) are gadolinium-based contrast agents combining the properties of conventional extracellular and liver-specific agents as they are both taken up by hepatocytes [5–7]. However, Gd-BOPTA and gadoxetate differ in their uptake by hepatocytes and subsequent biliary excretion [8–12].

While LI-RADS promotes standardisation for liver lesion characterisation, it primarily relies upon qualitative imaging features, many of which are subject to inter-reader variability and challenges related to background liver disease. Quantitative approaches to characterise focal lesions have been used successfully in other cancers such as breast [13] and prostate [14] and may be an avenue to improve standardisation for liver imaging as well.

In addition to liver lesion detection and characterisation with magnetic resonance imaging (MRI), the use of dynamic contrast-enhanced (DCE) MRI provides information on tissue characteristics by allowing noninvasive quantification of tissue perfusion and permeability. In the liver, pharmacokinetic modelling of dynamic time–signal intensity data from pre- and post-contrast imaging is used to calculate arterial flow ( $F_a$ ), portal venous flow

( $F_p$ ), arterial fraction (ART), mean transit time (MTT), and distribution volume (DV) of gadolinium-based contrast agents in the tissue of interest [15]. These features have been used to assess liver fibrosis, quantify vasculature characteristics and treatment response of HCC and liver metastases [15–21].

The vascular input function, particularly the arterial input function (AIF), is essential for perfusion quantification using pharmacokinetic modelling in the liver tumours. The size and shape of the AIF depend on the patient’s related factors such as heart rate and blood volume. Therefore, it is important to measure individual patient’s AIF to gain certainties in estimated physiological quantities, even if population-based AIF has been proposed [22]. Contrast agent perfusion dynamics in HCC and liver parenchyma with gadoxetate and Gd-BOPTA are not fully understood and studies investigating this topic with DCE-MRI are limited [23–25].

The objective of this study was (1) to assess the quality of the AIF during DCE-MRI of the liver and (2) to quantify perfusion parameters of HCC and liver parenchyma during dynamic phases (up to 180s) with DCE-MRI using gadoxetate and Gd-BOPTA in different patient populations.

## Materials and methods

This HIPAA compliant single-centre study was approved by the institutional review board and written informed consent was obtained for all patients. This was a retrospective evaluation of MRI studies acquired prospectively.

### Study population

We enrolled consecutive patients diagnosed with HCC by routine imaging who underwent DCE-MRI with Gd-BOPTA from June 2013 to August 2016 and patients who underwent DCE-MRI with gadoxetate from July to December 2016. Inclusion criteria were (1) age older than 18 years, (2) no contraindication for MRI or gadolinium-based contrast agents, (3) suspicion for HCC based on imaging findings, and (4) reference standard of histopathology or composite reference standard consisting of MRI features (LI-RADS) and multidisciplinary tumour board decision. A total of 71 patients with focal liver lesions compatible with HCC (based on previous imaging) were prospectively enrolled for a DCE-MRI study using gadoxetate (group 1) or Gd-BOPTA (group 2) for research purposes. Patients with inadequate image quality due to major motion artefacts ( $n = 1$  with gadoxetate,  $n = 3$  with Gd-BOPTA) and diagnoses other than HCC on pathology ( $n = 1$  lesion with Gd-BOPTA diagnosed as intrahepatic cholangiocarcinoma) were excluded. For all liver lesions included in this study, a LI-RADS v2018 score was assessed by one radiologist (D.S., 6 years of experience in cross-sectional imaging). Some participants ( $n = 42$ ) have been used in our previous studies on multiparametric MRI in HCC

[18, 26–28]. However, the data used in this study was not reported in any of these previously published studies.

## MRI technique

Before DCE-MRI acquisition, a  $T_1$ -weighted inversion recovery Look–Locker pulse sequence (180° inversion with 32 post inversion acquisitions) was used to provide quantitative  $T_1$  mapping in 1–2 slices through each lesion in one 18-s breath-hold.

The MRI acquisition was performed at 1.5 T (Aera, Siemens Healthineers;  $n = 52$ ) or 3.0T (Skyra ( $n = 6$ ) or BioGraph mMR ( $n = 8$ ), Siemens Healthineers), each equipped with a 32-channel spine and flexible 18-channel body array coil system.

The MRI protocols for gadoxetate (Eovist/Primovist®, Bayer Healthcare; 0.025 mmol/kg of body weight) and Gd-BOPTA (MultiHance®, Bracco, 0.05 mmol/kg of body weight) group were similar, except for the presence of fat suppression for the DCE-MRI sequence with gadoxetate. Details on MRI protocols can be found in [Supplementary Material](#) and Table 1.

Since we were interested in perfusion quantification during the dynamic phases, only images of the first 3 min after contrast agent administration were used for analysis.

## Arterial input function—qualitative assessment

The study coordinator (D.S., a radiologist with 6 years of experience) placed free-hand regions of interest (ROIs) on multiple consecutive slices in the abdominal

**Table 1** MR acquisition parameters for the  $T_1$  mapping sequence and the DCE-MRI sequence

	$T_1$ mapping	DCE-MRI
Sequence type	IR-LL	3D Flash
Acquisition plane	Axial	Axial
TE [ms]	1.04	1
TR [ms]	2.25	2.7–2.91
TI [ms]	42–1576.5	-
Flip angle [°]	8	9.5–11.5
Fat suppression	No	Only in group 1 (gadoxetate)
Field of view [mm <sup>2</sup> ]	420 × 288	380 × 280
Matrix	128 × 88	384 × 288 or 256 × 166
Slice thickness [mm]	8	4
Number of slices	1–2	40
Acceleration factor	2	4
Temporal resolution [s]	-	2–4

Abbreviations: IR-LL,  $T_1$ -weighted inversion recovery Look–Locker; TE, echo time; TR, repetition time; TI, inversion time

aorta at the level of the celiac trunk on unregistered DCE-MRI images for each patient using FireVoxel (CAI2R, New York University). The signal intensity (SI) of these ROIs was extracted for each time point of the DCE-MRI and subsequently exported for further data analysis to MATLAB (The MathWorks, Inc.). An AIF curve for the initial 180 s for each patient was calculated using a self-programmed MATLAB script.

After mutual training in 10 patients that were not part of the initial cohort, one radiologist (observer 1, N.V.V., 5 years of experience) and one physicist (observer 2, O.B., 6 years of experience in MRI research), blinded to the contrast agent used, independently evaluated the quality of the AIF curve for each patient. Both observers rated the following features for each AIF curve on a 3-point Likert scale: upslope, peak shape, peak width, downslope, recirculation peak, noise, and artefacts ([Supplementary Material](#)). A total additive score composed of each score for each AIF curve feature was calculated (score range 6–18).

## Arterial input function—reproducibility and test-retest repeatability of quantitative assessment

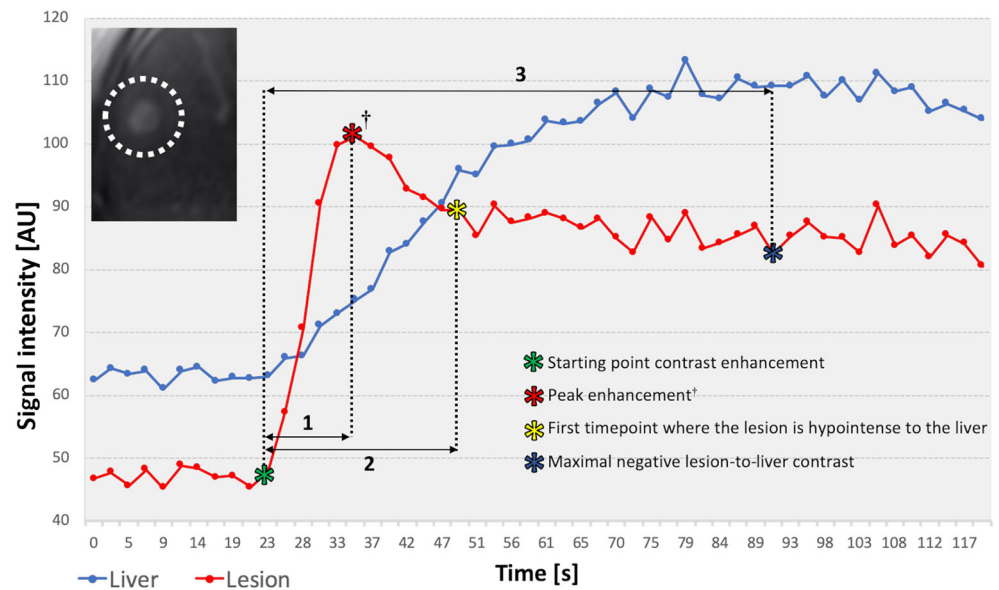
A description of AIF reproducibility and test-retest repeatability assessment can be found in the [Supplementary Material](#).

## Model-free parameters and lesion-to-liver contrast ratios

Model-free parameters were assessed to understand contrast agent dynamics in HCCs and to assess differences between the 2 agents. The study coordinator (D.S.) placed ROIs on multiple consecutive slices of registered DCE-MR images covering the index tumours and sparing the lesion capsule (when present), and on multiple slices in the adjacent liver parenchyma away from tumours (typical ROI size per slice approximately 2 cm<sup>2</sup>) avoiding large intrahepatic vessels and artefacts using FireVoxel software. Additionally, a ROI was placed in the portal vein on multiple slices. The SI of these ROIs was extracted for each time point of the DCE-MRI and subsequently exported for further data analysis to MATLAB. Six model-free parameters were calculated for the initial 3 min after contrast agent administration for all tumours: (1) time to peak enhancement, (2) time to washout, (3) maximal positive liver-to-contrast ratio (LLCR), (4) maximal negative LLCR, (5) time to maximal positive LLCR, (6) time to maximal negative LLCR (adapted from [29]). LLCR assesses lesion conspicuity during different phases and was defined as:

$$LLCR = \frac{SI_{lesion} - SI_{liver}}{SI_{liver}} \times 100\%$$

**Fig. 1** Measurements of model-free parameters in a 57-year-old male patient with HCC. DCE-MRI enhancement curves in HCC (red line) and liver parenchyma (blue line) with Gd-BOPTA. 1—HCC TTP enhancement, 2—HCC time to washout, and 3—time to maximal negative LLCR. In this case, the peak enhancement corresponds to the maximal positive lesion-to-liver contrast ratio<sup>†</sup>. Abbreviations: DCE-MRI, dynamic contrast-enhanced magnetic resonance imaging; HCC, hepatocellular carcinoma; Gd-BOPTA, gadobenate dimeglumine; LLCR, lesion-to-liver contrast ratio; TTP, time to peak; AU, arbitrary units; s, seconds



A detailed description of these parameters can be found in the [Supplementary Material](#) and measurements of the model-free parameters are summarised in Fig. 1.

## Modelled parameters

Data from the first 3 min after contrast injection was used for pharmacokinetic modelling. Average dynamic SI curves in the HCC, liver, aorta, and portal vein ROIs were converted to dynamic contrast agent concentration (CA) using the signal equation for a spoiled gradient recalled echo sequence, the pre-contrast  $T_1$  values, and the contrast agent's relaxivity. Average pre-contrast  $T_1$  values in HCCs and liver parenchyma were determined from the  $T_1$ -weighted IR-LL sequence. For the portal vein and aorta, pre-contrast  $T_1$  values were based on the literature [30]. A fixed haematocrit value of 0.45 was used for conversion from blood (CA) to plasma (CA) as described before [31, 32]. DCE-MRI modelling based on the average signal curve in the ROIs of HCCs and liver parenchyma was performed using a previously described dual-input single-compartment model [15, 18, 27, 33]. The following DCE-MRI parameters were estimated in the liver and HCCs: arterial flow ( $F_a$ ), portal venous flow ( $F_p$ ), total flow ( $F_t$ ), arterial fraction (ART), mean transit time (MTT), and distribution volume (DV).

## Statistical analysis

Continuous data are reported as mean  $\pm$  standard deviation (SD) or median with interquartile range (IQR) in parenthesis (1<sup>st</sup> percentile–3<sup>rd</sup> percentile). Categorical data are reported as frequencies with percentages in parenthesis. Inter-reader agreement for AIF curve features was assessed using the intra-class correlation

coefficient (ICC, two-way mixed model with absolute agreement). An ICC of 0.91–1.00 indicated excellent, 0.75–0.90 good, 0.50–0.74 fair, and  $< 0.5$  poor agreement [34, 35]. To evaluate the reproducibility and test-retest repeatability of AIF quantitative curve features, we calculated the coefficient of variation [ $CV = (\text{standard deviation}/\text{mean}) \times 100$ ]. Reproducibility/repeatability of AIF parameters was considered excellent if  $CV < 10\%$ , acceptable if  $CV = 10\text{--}20\%$ , modest if  $CV = 20.1\text{--}40\%$ , and poor if  $CV > 40\%$ . To evaluate differences in study population characteristics, modelled and model-free parameters between groups 1 and 2, Fisher's exact tests were used for dichotomous variables and Mann-Whitney  $U$  tests for independent scaled variables. Additionally, we calculated  $R^2$  to assess the goodness-of-fit for the pharmacokinetic model. In patients with repeat measurements, the baseline DCE-MRI parameters were used for the analysis. No power analysis was performed for this study. All statistical analyses were performed using SPSS (IBM® SPSS® Statistics 20; SPSS® Inc.) and were two-tailed.  $p < 0.05$  was considered statistically significant.

## Results

### Study population

The final study population consisted of 66 patients with 83 HCCs. Twenty-eight patients (21M/7F; mean age 66.8  $\pm$  10.8 years; BMI 28.6  $\pm$  6.0 kg/m<sup>2</sup>) with 34 HCCs underwent DCE-MRI with gadoxetate (group 1) and 38 patients (30M/8F; mean age 60.9  $\pm$  9.5 years; BMI 27.6  $\pm$  4.6 kg/m<sup>2</sup>) with 49 HCCs underwent DCE-MRI with Gd-BOPTA (group 2). Detailed results regarding the study population can be found in Table 2 and in [Supplementary Material](#).

**Table 2** Study population characteristics

Characteristic	Group 1 (gadoxetate) (n = 28)	Group 2 ( Gd-BOPTA) (n = 38)	p
Mean age (y) <sup>†</sup>	66.8 ± 10.8	60.9 ± 9.5	0.001
Gender (female/male)*	7/21	8/30	> 0.9
BMI (kg/m <sup>2</sup> ) <sup>†</sup>	28.6 ± 6.0	27.6 ± 4.6	0.006
Cirrhosis*	25 (89.3)	30 (78.9)	> 0.9
Child-Pugh score*			0.413
A	15 (60.0)	21 (70.0)	-
B	9 (36.0)	8 (26.7)	-
C	1 (4.0)	1 (3.3)	-
Aetiology of liver disease*			0.194
HCV infection	17 (60.7)	21 (55.3)	
HBV infection	2 (7.1)	11 (28.9)	
NASH	5 (17.9)	3 (7.9)	
Alcohol intoxication	3 (10.7)	2 (5.3)	
No risk factor	1 (3.6)	1 (2.6)	

Fisher's exact tests were used for dichotomous variables, Mann-Whitney *U* tests for independent scaled variables and chi-Square test for independent nominal data

Abbreviations: HCV, hepatitis C virus; HBV, hepatitis B virus; NASH, nonalcoholic steatohepatitis; HCC, hepatocellular carcinoma

\*Data are numbers of patients with percentages in parentheses

<sup>†</sup>Data are numbers of patients with standard deviations in parentheses

## AIF—quality assessment

The score for the recirculation peak was significantly lower in group 1 compared to group 2 ( $p < 0.001$ ) while the score for noise and artefacts was significantly higher with group 1 ( $p < 0.001$ ). However, the total score for AIF quality was similar for the two groups ( $p = 0.818$ ) (Table 3, Fig. 2). Inter-reader agreement was good for the total qualitative score (ICC = 0.88).

Results from AIF reproducibility and test-retest repeatability assessment of quantitative features can be found in the [Supplementary Material](#) and [Supplementary Table 1](#).

## Model-free parameters and LLCR

No significant differences in model-free parameters (time to peak, time to washout) and maximal positive and negative LLCR were observed in HCCs between the two groups (all  $p = 0.054$ – $0.398$ ). Liver TTP and time to maximal negative LLCR were significantly longer with group 1 compared to group 2, due to delayed enhancement of the liver (Table 4, Fig. 3). There was no significant difference in the time to maximal positive LLCR between the two groups ( $p = 0.471$ ) (Fig. 4).

**Table 3** Qualitative assessment of arterial input function results for two independent observers. Mann-Whitney *U* test was used to compare the 2 groups and intra-class correlation coefficient (ICC) to assess inter-observer agreement

	Observer 1			Observer 2			ICC
	Group 1 (gadoxetate)	Group 2 (Gd-BOPTA)	p	Group 1 (gadoxetate)	Group 2 (Gd-BOPTA)	p	
Upslope	3.0 ± 0.2	3.0 ± 0.2	0.221	2.5 ± 0.6	2.8 ± 0.4	<b>0.028</b>	0.07
Peak shape	2.4 ± 0.8	2.1 ± 0.8	<b>0.042</b>	2.4 ± 0.8	2.3 ± 0.7	0.755	0.77
Peak width	2.5 ± 0.7	2.6 ± 0.8	0.288	2.5 ± 0.7	2.3 ± 0.8	0.305	0.84
Downslope	2.2 ± 0.7	2.2 ± 0.7	0.983	2.2 ± 0.7	2.1 ± 0.7	0.673	0.88
Recirculation peak	1.3 ± 0.6	2.5 ± 0.6	<b>&lt; 0.001</b>	1.7 ± 0.8	2.6 ± 0.5	<b>&lt; 0.001</b>	0.86
Noise/artefacts	2.5 ± 0.5	1.7 ± 0.6	<b>0.001</b>	2.7 ± 0.5	1.7 ± 0.6	<b>0.001</b>	0.88
Total score	14.0 ± 2.2	14.1 ± 2.2	0.818	14.0 ± 2.2	14.0 ± 2.4	0.932	0.88

Statistically significant results are marked in bold



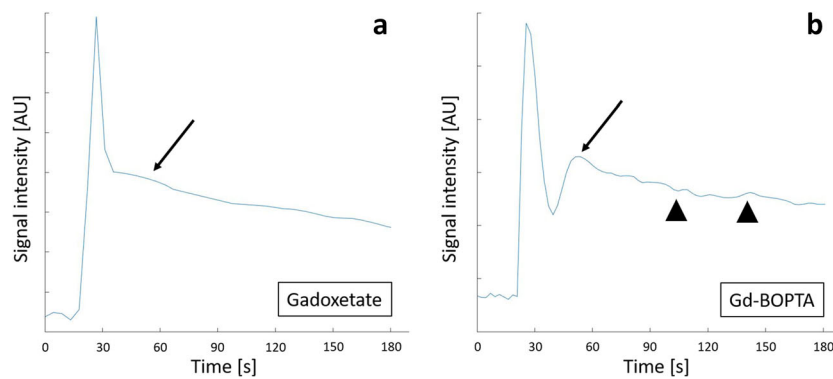


**Fig. 2** Example of AIF curves measured in the abdominal aorta with gadoxetate (a) and Gd-BOPTA (b) in two different patients with HCC. On the AIF curve with Gd-BOPTA, a recirculation peak is seen (arrow in b) while there was no visible recirculation peak with gadoxetate (arrow in a). Furthermore, the AIF curve with Gd-BOPTA shows minor noise and

artefacts (arrowheads in b) while there was no irregularities related to noise and artefacts in the AIF curve with gadoxetate. Abbreviations: AIF, arterial input function; HCC, hepatocellular carcinoma; Gd-BOPTA, gadobenate dimeglumine; AU, arbitrary units; s, seconds

**Modelled perfusion parameters**

*HCC:* No significant differences between the two groups were observed for  $F_a$ ,  $F_p$ ,  $F_t$ , ART, MTT, and DV ( $p = 0.222–0.810$ ), with similar median  $R^2$  ( $p = 0.439$ ).

*Liver:*  $F_p$  and  $F_t$  were significantly lower in group 1 compared to those in group 2 ( $p = 0.002$  and  $p = 0.001$ , respectively). Liver MTT was significantly longer for group 1 compared to that for group 2 ( $p < 0.001$ ). No significant differences between the two groups were found for  $F_a$ , ART, and DV ( $p = 0.344–0.736$ ). The median  $R^2$  was significantly lower for group 1 ( $p = 0.013$ ) (Table 5).

**Discussion**

This study of quantitative DCE-MRI perfusion showed overall similar AIF quality and perfusion parameters in HCCs during the dynamic phases (within 3 min after contrast agent injection) using gadoxetate (group 1) vs Gd-BOPTA (group 2) in two different patient populations. However, significant differences were

observed for the time to maximal negative LLCR, which was longer in group 1 compared to group 2, explained by decreased and delayed enhancement of the liver in group 1. This could translate into different post-contrast imaging time points to obtain the highest lesion conspicuity. Of note, LLCRs were not different between groups, implying no difference in lesion conspicuity between the 2 agents, despite differences in injected contrast dose.

We found a similar overall quality score for AIF curves measured in the abdominal aorta with both contrast agents. However, the score was significantly lower for the recirculation peak of AIF curves and significantly higher for noise and artefacts for group 1 compared to group 2. Since the administered volume was the same for both contrast agents (0.1 mL/kg), the recirculation peak with Gd-BOPTA could be explained by the higher dose of administered gadolinium (0.05 mmol/kg) compared to gadoxetate (0.025 mmol/kg) which leads to a higher  $T_1$  relaxation rate in plasma [36]. Furthermore, the injection rate in group 1 was slower compared to that in group 2, which might have partially contributed to the differences in these parameters. Overall, we believe that both contrast agents are suitable for DCE-MRI with regards to AIF quality.

**Table 4** Model-free perfusion parameters in HCC and liver parenchyma and lesion-to-liver contrast ratios on both groups. Data is presented as numbers or mean ± standard deviation

	Group 1 (Gadoxetate)	Group 2 (Gd-BOPTA)	$p^*$
Number of Lesions [n]	33	48	-
Time to peak HCC [s]	26.2 ± 12.4	30.6 ± 18.4	0.398
Time to washout [s]	53.0 ± 24.2	40.1 ± 13.7	0.054
Time to peak liver [s]	135.3 ± 50.2	83.5 ± 37.4	<b>&lt; 0.001</b>
Max. positive LLCR [%]	33.9 ± 29.6	39.2 ± 29.8	0.230
Time to max. positive LLCR [s]	16.5 ± 6.5	15.8 ± 4.8	0.471
Max. negative LLCR [%]	-15.1 ± 17.9	-11.0 ± 20.3	0.317
Time to max. negative LLCR [s]	162.9 ± 25.9	115.0 ± 39.0	<b>&lt; 0.001</b>

Statistically significant results are marked in bold

Abbreviations: LLCR, lesion-to-liver contrast ratio; HCC, hepatocellular carcinoma

\*Mann-Whitney  $U$  test

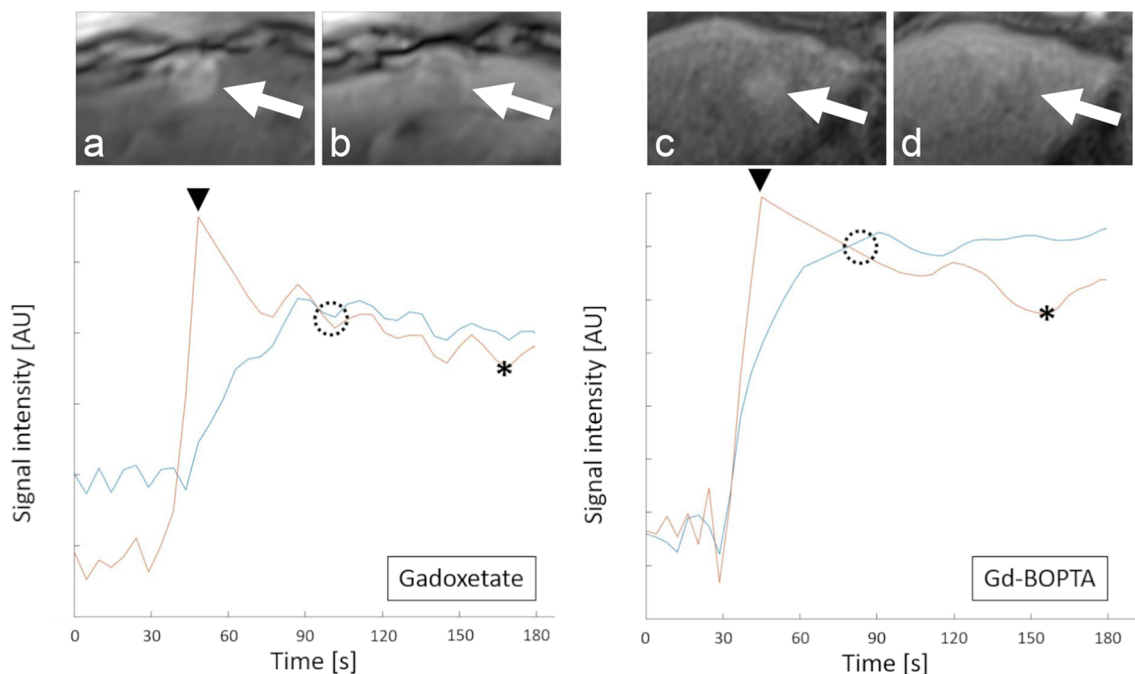


**Fig. 3** Example of DCE-MRI enhancement curves of HCC (orange line) and liver parenchyma (blue line) in a 70-year-old male who received gadoxetate and a 63-year-old female who received Gd-BOPTA. Both HCCs show arterial phase hyperenhancement (a and c, peak enhancement indicated by the arrowhead on the enhancement curve) and washout (b and d, dashed circle on the enhancement curve). TTP, time to washout

and time to maximal negative LLCR (asterisk on the enhancement curve) were 13.4, 66.3 and 142.1 s for gadoxetate; and 19.4, 67.8 and 154.1 s for Gd-BOPTA. Abbreviations: DCE-MRI, dynamic contrast-enhanced magnetic resonance imaging; HCC, hepatocellular carcinoma; LLCR, lesion-to-liver contrast ratio; Gd-BOPTA, gadobenate dimeglumine; AU, arbitrary units; s, seconds

We did not find significant differences in the time to peak and washout in HCCs as well as maximal positive and negative LLCR between the two groups. These findings might indicate that the lesion conspicuity in the arterial portal venous and transitional/delayed phases may be similar for both

contrast agents. The significantly shorter time to maximal negative LLCR in group 2 could be related to faster liver enhancement, indicated by a shorter liver MTT and TTP. Some of our patients had liver cirrhosis, which potentially reduces the uptake of these agents in the hepatocytes [23,

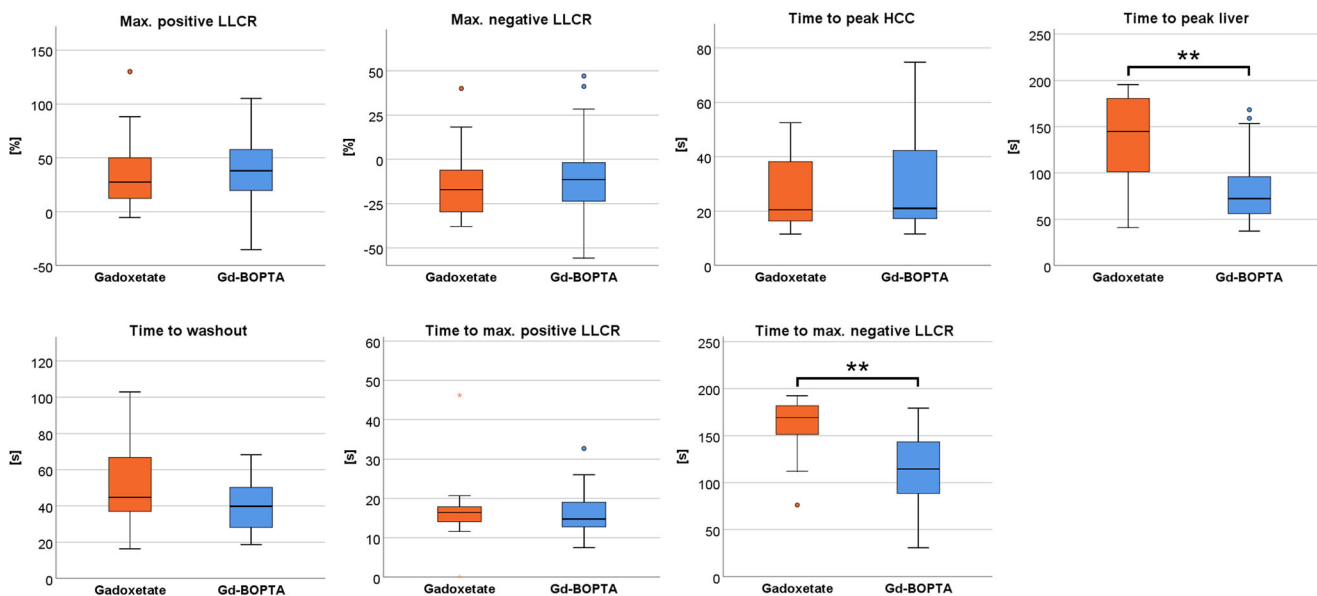


**Fig. 4** Boxplots of model-free parameters and lesion-to-liver contrast ratio parameters measured in HCC and liver parenchyma with DCE-MRI with gadoxetate and Gd-BOPTA. Abbreviations: DCE-MRI,

dynamic contrast-enhanced magnetic resonance imaging; HCC, hepatocellular carcinoma; LLCR, lesion-to-liver contrast ratio; Gd-BOPTA, gadobenate dimeglumine. \*\*  $p < 0.001$

**Table 5** Modelled perfusion parameters in HCC and liver parenchyma in both groups. Data is presented as median with interquartile range in parenthesis

	Liver		HCC			
	Group 1 (gadoxetate)	Group 2 (Gd-BOPTA)	<i>p</i> *	Group 1 (gadoxetate)	Group 2 (Gd-BOPTA)	<i>p</i> *
$F_a$ [mL/100g/min]	15.4 (4.1–39.3)	18.8 (10.0–34.8)	0.460	59.1 (41.8–94.8)	70.0 (39.7–156.5)	0.598
$F_p$ [mL/100g/min]	73.8 (51.7–91.5)	120.5 (76.7–199.6)	<b>0.002</b>	36.3 (5.1–211.5)	36.1 (2.3–117.0)	0.590
$F_t$ [mL/100g/min]	87.9 (69.4–136.3)	150.7 (105.8–265.6)	<b>0.001</b>	126.9 (65.3–299.1)	117.1 (72.0–357.0)	0.810
ART [%]	15.5 (5.7–41.7)	11.4 (5.7–25.6)	0.344	66.3 (23.3–91.3)	76.8 (43.8–95.8)	0.409
MTT [s]	32.5 (22.0–51.9)	16.5 (12.1–24.1)	<b>&lt; 0.001</b>	13.2 (2.6–26.2)	16.8 (8.0–29.1)	0.384
DV [%]	54.4 (33.2–62.4)	42.4 (33.3–68.6)	0.736	24.0 (18.2–32.4)	28.7 (21.0–37.1)	0.222
$R^2$ [AU]	0.974 (0.964–0.982)	0.982 (0.976–0.997)	<b>0.013</b>	0.940 (0.859–0.954)	0.932 (0.813–0.948)	0.439

Abbreviations:  $F_a$ , arterial flow;  $F_p$ , portal flow;  $F_t$ , total flow; ART, arterial fraction; MTT, mean transit time; DV, distribution volume; HCC, hepatocellular carcinoma

Statistically significant results are marked in bold

\*Mann-Whitney *U* test

37]. However, despite the fact that gadoxetate and Gd-BOPTA are classified as liver-specific agents, we believe that during the dynamic phases the perfusion dynamics in HCC and liver parenchyma with these agents are similar to extracellular agents with minimal hepatocyte uptake (especially for Gd-BOPTA).

Our pharmacokinetic parameters of the liver and HCC were in similar range as previously reported [21, 25, 38]. In our study, the significantly lower  $F_p$  and  $F_t$  in the liver in group 1 may be explained by the slightly higher percentage of cirrhotic patients in group 1 (89.3% vs 78.9% in group 2) since liver flow is influenced by cirrhosis with a shift from predominantly portal venous inflow to predominantly arterial inflow as cirrhosis develops [39]. However, the incidence of cirrhosis and the Child-Pugh class did not show significant differences between the two groups. The higher contrast agent concentration in the blood when Gd-BOPTA was used might also have contributed to a higher portal venous and consequently total hepatic flow. We found a significantly longer liver MTT in group 1. Since MTT is calculated as blood volume divided by blood flow, we assume that the differences in  $F_p$  and  $F_t$  between the two groups are responsible for the differences in MTT. Furthermore, it has been reported that the injection rate influences perfusion parameters [40] and AIF shape [41]. Therefore, we hypothesise that the differences in the injection rate may have also contributed to the differences in the hepatic flow [40].

The curve fitting ( $R^2$ ) for the pharmacokinetic models was high for both groups in the liver and in HCCs, indicating good fit quality for the used model. However,  $R^2$  values were

slightly higher for the pharmacokinetic model in the liver compared to HCCs. These findings are similar to previously published results [27], indicating that fitting is improved in the liver. A possible explanation for this is that lesions are more susceptible to motion, resulting in worse data quality for DCE-MRI.

DCE-MRI provides quantitative information about liver and tumour perfusion and allows for assessment of vascular characteristics and treatment response of HCCs [15, 18, 19, 21]. Data on DCE-MRI using gadoxetate is limited [23, 42–44]. In our study, the use of gadoxetate did not affect perfusion quantification in HCCs compared to Gd-BOPTA, while it may increase sensitivity in the detection of liver lesions in the hepatobiliary phase [45, 46].

We believe that DCE-MRI can be used with gadoxetate or Gd-BOPTA with the benefit of higher lesion-to-liver contrast during the HBP associated with liver-specific agents, although this was not assessed here. Recent studies suggested that perfusion parameters obtained with liver-specific agents could be used as biomarkers for early prediction of therapeutic outcome in HCCs after transarterial chemoembolisation or radioembolisation [17, 25]. Besides the advantages of liver-specific agents in terms of lesion detection, it has been shown that gadoxetate DCE-MRI allows quantification of drug-induced alterations in hepatobiliary transporter activity and has the potential to serve as a biomarker of liver function [42, 43]. However, data on DCE-MRI using liver-specific contrast agents is still sparse and future studies are needed to assess its added value for lesion characterisation, therapy response, and liver function evaluation.



Our study has several limitations. First, we did not compare an extracellular agent with a liver-specific agent but two different liver-specific agents. However, we assessed the perfusion during the initial dynamic phases, with limited effect of hepatocyte uptake on HCC perfusion. Second, we did not perform a cross-over study (in which both contrast agents are used in the same patient population), which would have been ideal, but more challenging to conduct. Third, the MRI acquisition was slightly different between both groups. In particular, the differences in injection rate may have induced some differences in the AIF quality. Fourth, some patients had more than one lesions, which might have led to “clustering” effects in the statistical analysis. However, since the percentage of patients with multiple lesions was rather small, we assume that “clustering” effects might be negligible.

We conclude that gadoxetate and Gd-BOPTA provide comparable AIF quality and perfusion parameters in HCC during the dynamic phases (first 3 min post injection). Despite delayed and decreased liver enhancement with gadoxetate disodium, the lesion-to-liver contrast ratios were equivalent for both contrast agents with slightly different timing, indicating similar lesion conspicuity for both contrast agents with different post-contrast imaging time points to obtain the highest lesion conspicuity.

**Supplementary Information** The online version contains supplementary material available at <https://doi.org/10.1007/s00330-021-08068-5>.

**Funding** This study was funded by the National Cancer Institute (NCI grant 1U01CA172320).

## Declarations

**Guarantor** The scientific guarantor of this publication is Bachir Taouli.

**Conflict of interest** The authors of this manuscript declare relationships with the following companies:

Kathryn J. Fowler:  
 Research grants: Bayer Healthcare, GE, Pfizer  
 Consulting: Epigenomics, 12 Sigma, Medscape, Bayer Healthcare  
 Claude B. Sirlin:  
 Industry research support: Bayer Healthcare, GE, Gilead, Philips, Siemens  
 Consulting: Epigenomics  
 Institutional Consulting Representative: IBM-Watson  
 Bachir Taouli:  
 Research grants: Bayer Healthcare, Takeda  
 Consultant: Bayer Healthcare, Alexion  
 All other authors declare no conflict of interest.

**Statistics and biometry** One of the authors (Stefanie Hectors) has significant statistical expertise.

**Informed consent** Written informed consent was obtained from all subjects (patients) in this study.

**Ethical approval** Institutional Review Board approval was obtained.

**Study subjects or cohorts overlap** Some participants ( $n=42$ ) have been used in our previous studies on multiparametric MRI in HCC:

1Bane O, Besa C, Wagner M et al (2016) Feasibility and reproducibility of BOLD and TOLD measurements in the liver with oxygen and carbogen gas challenge in healthy volunteers and patients with hepatocellular carcinoma. *J Magn Reson Imaging* 43:866–876

2Hectors SJ, Wagner M, Bane O et al (2017) Quantification of hepatocellular carcinoma heterogeneity with multiparametric magnetic resonance imaging. *Sci Rep* 7:2452

3Hectors SJ, Wagner M, Besa C et al (2016) Intravoxel incoherent motion diffusion-weighted imaging of hepatocellular carcinoma: is there a correlation with flow and perfusion metrics obtained with dynamic contrast-enhanced MRI? *J Magn Reson Imaging* 44:856–864

4Jajamovich GH, Huang W, Besa C et al (2016) DCE-MRI of hepatocellular carcinoma: perfusion quantification with Tofts model versus shutter-speed model—initial experience. *MAGMA* 29:49–58

## Methodology

- prospective
- cross-sectional study
- performed at one institution

## References

1. European Association for the Study of the Liver (2018) EASL Clinical Practice Guidelines: Management of hepatocellular carcinoma. Management of hepatocellular carcinoma. *J Hepatol* 69: 182–236
2. Marrero JA, Kulik LM, Sirlin CB et al (2018) Diagnosis, staging, and management of hepatocellular carcinoma: 2018 Practice Guidance by the American Association for the Study of Liver Diseases. *Hepatology* 68:723–750
3. Omata M, Cheng AL, Kokudo N et al (2017) Asia-Pacific clinical practice guidelines on the management of hepatocellular carcinoma: a 2017 update. *Hepatol Int* 11:317–370
4. American College of Radiology Liver Imaging Reporting and Data System. 2019. Available via <https://www.acr.org/Clinical-Resources/Reporting-and-Data-Systems/LI-RADS>. Accessed 23 May 2019
5. Reimer P, Rummeny EJ, Shamsi K et al (1996) Phase II clinical evaluation of Gd-EOB-DTPA: dose, safety aspects, and pulse sequence. *Radiology* 199:177–183
6. Spinazzi A, Lorusso V, Pirovano G, Kirchin M (1999) Safety, tolerance, biodistribution, and MR imaging enhancement of the liver with gadobenate dimeglumine: results of clinical pharmacologic and pilot imaging studies in nonpatient and patient volunteers. *Acad Radiol* 6:282–291
7. Kirchin MA, Pirovano GP, Spinazzi A (1998) Gadobenate dimeglumine (Gd-BOPTA). An overview. *Invest Radiol* 33:798–809
8. Carlos RC, Branam JD, Dong Q, Hussain HK, Francis IR (2002) Biliary imaging with Gd-EOB-DTPA: is a 20-minute delay sufficient? *Acad Radiol* 9:1322–1325
9. Carlos RC, Hussain HK, Song JH, Francis IR (2002) Gadolinium-ethoxybenzyl-diethylenetriamine pentaacetic acid as an intrabiliary contrast agent: preliminary assessment. *AJR Am J Roentgenol* 179: 87–92
10. Schuhmann-Giampieri G, Schmitt-Willich H, Press WR, Negishi C, Weinmann HJ, Speck U (1992) Preclinical evaluation of Gd-EOB-DTPA as a contrast agent in MR imaging of the hepatobiliary system. *Radiology* 183:59–64

11. Vogl TJ, Kummel S, Hammerstingl R et al (1996) Liver tumors: comparison of MR imaging with Gd-EOB-DTPA and Gd-DTPA. *Radiology* 200:59–67
12. Petersein J, Spinazzi A, Giovagnoni A et al (2000) Focal liver lesions: evaluation of the efficacy of gadobenate dimeglumine in MR imaging—a multicenter phase III clinical study. *Radiology* 215:727–736
13. El Khouli RH, Macura KJ, Jacobs MA et al (2009) Dynamic contrast-enhanced MRI of the breast: quantitative method for kinetic curve type assessment. *AJR Am J Roentgenol* 193:W295–W300
14. Vargas HA, Akin O, Franiel T et al (2011) Diffusion-weighted endorectal MR imaging at 3 T for prostate cancer: tumor detection and assessment of aggressiveness. *Radiology* 259:775–784
15. Materne R, Smith AM, Peeters F et al (2002) Assessment of hepatic perfusion parameters with dynamic MRI. *Magn Reson Med* 47:135–142
16. Abdullah SS, Pialat JB, Wiart M et al (2008) Characterization of hepatocellular carcinoma and colorectal liver metastasis by means of perfusion MRI. *J Magn Reson Imaging* 28:390–395
17. Hectors SJ, Lewis S, Kennedy P et al (2020) Assessment of hepatocellular carcinoma response to (90)Y radioembolization using dynamic contrast material-enhanced MRI and intravoxel incoherent motion diffusion-weighted imaging. *Radiol Imaging Cancer* 2:e190094
18. Hectors SJ, Wagner M, Bane O et al (2017) Quantification of hepatocellular carcinoma heterogeneity with multiparametric magnetic resonance imaging. *Sci Rep* 7:2452
19. Hsu CY, Shen YC, Yu CW et al (2011) Dynamic contrast-enhanced magnetic resonance imaging biomarkers predict survival and response in hepatocellular carcinoma patients treated with sorafenib and metronomic tegafur/uracil. *J Hepatol* 55:858–865
20. Miyazaki K, Orton MR, Davidson RL et al (2012) Neuroendocrine tumor liver metastases: use of dynamic contrast-enhanced MR imaging to monitor and predict radiolabeled octreotide therapy response. *Radiology* 263:139–148
21. Taouli B, Johnson RS, Hajdu CH et al (2013) Hepatocellular carcinoma: perfusion quantification with dynamic contrast-enhanced MRI. *AJR Am J Roentgenol* 201:795–800
22. Parker GJ, Roberts C, Macdonald A et al (2006) Experimentally-derived functional form for a population-averaged high-temporal-resolution arterial input function for dynamic contrast-enhanced MRI. *Magn Reson Med* 56:993–1000
23. Juluru K, Talal AH, Yantiss RK et al (2017) Diagnostic accuracy of intracellular uptake rates calculated using dynamic Gd-EOB-DTPA-enhanced MRI for hepatic fibrosis stage. *J Magn Reson Imaging* 45:1177–1185
24. Saito K, Ledsam J, Sugimoto K, Sourbron S, Araki Y, Tokuyue K (2018) DCE-MRI for early prediction of response in hepatocellular carcinoma after TACE and sorafenib therapy: a pilot study. *J Belg Soc Radiol* 102:40
25. Thibodeau-Antonacci A, Petitclerc L, Gilbert G et al (2019) Dynamic contrast-enhanced MRI to assess hepatocellular carcinoma response to Transarterial chemoembolization using LI-RADS criteria: a pilot study. *Magn Reson Imaging* 62:78–86
26. Bane O, Besa C, Wagner M et al (2016) Feasibility and reproducibility of BOLD and TOLD measurements in the liver with oxygen and carbogen gas challenge in healthy volunteers and patients with hepatocellular carcinoma. *J Magn Reson Imaging* 43:866–876
27. Hectors SJ, Wagner M, Besa C et al (2016) Intravoxel incoherent motion diffusion-weighted imaging of hepatocellular carcinoma: is there a correlation with flow and perfusion metrics obtained with dynamic contrast-enhanced MRI? *J Magn Reson Imaging* 44:856–864
28. Jajamovich GH, Huang W, Besa C et al (2016) DCE-MRI of hepatocellular carcinoma: perfusion quantification with Tofts model versus shutter-speed model—initial experience. *MAGMA* 29:49–58
29. Taouli B, Sandberg A, Stemmer A et al (2009) Diffusion-weighted imaging of the liver: comparison of navigator triggered and breathhold acquisitions. *J Magn Reson Imaging* 30:561–568
30. Zhang X, Petersen ET, Ghariq E et al (2013) In vivo blood T(1) measurements at 1.5 T, 3 T, and 7 T. *Magn Reson Med* 70:1082–1086
31. Georgiou L, Penny J, Nicholls G et al (2017) Quantitative assessment of liver function using gadoxetate-enhanced magnetic resonance imaging: monitoring transporter-mediated processes in healthy volunteers. *Invest Radiol* 52:111–119
32. Li Z, Sun J, Chen L et al (2016) Assessment of liver fibrosis using pharmacokinetic parameters of dynamic contrast-enhanced magnetic resonance imaging. *J Magn Reson Imaging* 44:98–104
33. Aronhime S, Calcagno C, Jajamovich GH et al (2014) DCE-MRI of the liver: effect of linear and nonlinear conversions on hepatic perfusion quantification and reproducibility. *J Magn Reson Imaging* 40:90–98
34. Shrout PE, Fleiss JL (1979) Intraclass correlations: uses in assessing rater reliability. *Psychol Bull* 86:420–428
35. Koo TK, Li MY (2016) A guideline of selecting and reporting intraclass correlation coefficients for reliability research. *J Chiropr Med* 15:155–163
36. Pintaske J, Martirosian P, Graf H et al (2006) Relaxivity of gadopentetate dimeglumine (Magnevist), gadobutrol (Gadovist), and gadobenate dimeglumine (MultiHance) in human blood plasma at 0.2, 1.5, and 3 Tesla. *Invest Radiol* 41:213–221
37. Lee S, Choi D, Jeong WK (2016) Hepatic enhancement of Gd-EOB-DTPA-enhanced 3 Tesla MR imaging: assessing severity of liver cirrhosis. *J Magn Reson Imaging* 44:1339–1345
38. Patel J, Sigmund EE, Rusinek H, Oei M, Babb JS, Taouli B (2010) Diagnosis of cirrhosis with intravoxel incoherent motion diffusion MRI and dynamic contrast-enhanced MRI alone and in combination: preliminary experience. *J Magn Reson Imaging* 31:589–600
39. Kudo M (2009) Multistep human hepatocarcinogenesis: correlation of imaging with pathology. *J Gastroenterol* 44(Suppl 19):112–118
40. Aerts HJ, van Riel NA, Backes WH (2008) System identification theory in pharmacokinetic modeling of dynamic contrast-enhanced MRI: influence of contrast injection. *Magn Reson Med* 59:1111–1119
41. Sari H, Erlandsson K, Barnes A et al (2014) Modelling the impact of injection time on the bolus shapes in PET-MRI AIF Conversion. *EJNMMI Phys* 1:A54
42. Saito K, Ledsam J, Sourbron S et al (2013) Assessing liver function using dynamic Gd-EOB-DTPA-enhanced MRI with a standard 5-phase imaging protocol. *J Magn Reson Imaging* 37:1109–1114
43. Ulloa JL, Stahl S, Yates J et al (2013) Assessment of gadoxetate DCE-MRI as a biomarker of hepatobiliary transporter inhibition. *NMR Biomed* 26:1258–1270
44. Hectors SJ, Bane O, Kennedy P et al (2021) Noninvasive diagnosis of portal hypertension using gadoxetate DCE-MRI of the liver and spleen. *Eur Radiol*. <https://doi.org/10.1007/s00330-020-07495-0>
45. Ahn SS, Kim MJ, Lim JS, Hong HS, Chung YE, Choi JY (2010) Added value of gadoxetic acid-enhanced hepatobiliary phase MR imaging in the diagnosis of hepatocellular carcinoma. *Radiology* 255:459–466
46. Song JS, Choi EJ, Hwang SB, Hwang HP, Choi H (2019) LI-RADS v2014 categorization of hepatocellular carcinoma: Intraindividual comparison between gadopentetate dimeglumine-enhanced MRI and gadoxetic acid-enhanced MRI. *Eur Radiol* 29:401–410

**Publisher's note** Springer Nature remains neutral with regard to jurisdictional claims in published maps and institutional affiliations.